

CERN-EP-2023-145
24 July 2023

Improved measurement of CP violation parameters in $B_s^0 \rightarrow J/\psi K^+ K^-$ decays in the vicinity of the $\phi(1020)$ resonance

LHCb collaboration[†]

Abstract

The decay-time-dependent CP asymmetry in $B_s^0 \rightarrow J/\psi(\rightarrow \mu^+ \mu^-) K^+ K^-$ decays is measured using proton-proton collision data, corresponding to an integrated luminosity of 6 fb^{-1} , collected with the LHCb detector at a center-of-mass energy of 13 TeV. Using a sample of approximately 349 000 B_s^0 signal decays with an invariant $K^+ K^-$ mass in the vicinity of the $\phi(1020)$ resonance, the CP -violating phase ϕ_s is measured, along with the difference in decay widths of the light and heavy mass eigenstates of the B_s^0 - \bar{B}_s^0 system, $\Delta\Gamma_s$, and the difference of the average B_s^0 and B^0 meson decay widths, $\Gamma_s - \Gamma_d$. The values obtained are $\phi_s = -0.039 \pm 0.022 \pm 0.006 \text{ rad}$, $\Delta\Gamma_s = 0.0845 \pm 0.0044 \pm 0.0024 \text{ ps}^{-1}$ and $\Gamma_s - \Gamma_d = -0.0056 \pm_{-0.0015}^{+0.0013} \pm 0.0014 \text{ ps}^{-1}$, where the first uncertainty is statistical and the second systematic. These are the most precise single measurements to date and are consistent with expectations based on the Standard Model and with the previous LHCb analyses of this decay. These results are combined with previous independent LHCb measurements. The phase ϕ_s is also measured independently for each polarization state of the $K^+ K^-$ system and shows no evidence for polarization dependence.

Submitted to Phys. Rev. Lett.

© 2023 CERN for the benefit of the LHCb collaboration. CC BY 4.0 licence.

[†]Authors are listed at the end of this Letter.

The interference between B_s^0 -mixing and -decay amplitudes to CP eigenstates with a $c\bar{c}$ resonance in the final state gives rise to a measurable CP -violating phase, ϕ_s , which is particularly sensitive to physics beyond the Standard Model (SM). In the SM, neglecting subleading loop contributions in $b \rightarrow c\bar{c}s$ transitions, ϕ_s is predicted to be equal to $-2\beta_s$, where $\beta_s \equiv \arg[-(V_{ts}V_{tb}^*)/(V_{cs}V_{cb}^*)]$ and V_{ij} are elements of the Cabibbo-Kobayashi-Maskawa (CKM) quark-flavor-mixing matrix [1]. Global fits to experimental data, under the assumption of the CKM paradigm, give $-2\beta_s = -0.0368_{-0.0006}^{+0.0009}$ rad [2]. This precise indirect determination makes the measurement of ϕ_s an excellent probe for physics beyond the SM, especially for models contributing to B_s^0 - \bar{B}_s^0 mixing [3, 4]. Several experiments have measured ϕ_s , the B_s^0 decay width and decay-width difference, Γ_s and $\Delta\Gamma_s$, in B_s^0 decays via $b \rightarrow c\bar{c}s$ transitions [5–19]. The measurements lead to the current world average of $\phi_s^{c\bar{c}s} = -0.049 \pm 0.019$ rad [20], which is dominated by the LHCb results in $B_s^0 \rightarrow J/\psi h^+ h^-$ ($h = K, \pi$) decays using 5 fb^{-1} of data collected at center-of-mass energies of $\sqrt{s} = 7, 8$ and 13 TeV [13]. This Letter reports an update of the LHCb measurements in $B_s^0 \rightarrow J/\psi K^+ K^-$ decays¹ using the full Run 2 data taken in 2015–2018, corresponding to an integrated luminosity of 6 fb^{-1} at $\sqrt{s} = 13 \text{ TeV}$. The results supersede those in Ref. [13] and are combined with the LHCb result using 3 fb^{-1} of Run 1 data [12]. Apart from the increased data size, this analysis benefits from improvements in calibration of the particle identification (PID), flavor tagging algorithms, and the B_s^0 decay-time resolution model.

The LHCb detector is a single-arm forward spectrometer covering the pseudorapidity range $2 < \eta < 5$, described in details in Refs [21, 22]. Simulated events produced with the software described in Refs. [23–26] are used to model the effects of the detector acceptance, resolution, and selection requirements. Dedicated simulations are produced for each year of data-taking corresponding to the relevant detector and accelerator conditions. High-purity data samples of charm hadron, charmonia, and beauty hadron decays are used to calibrate the simulated single-particle reconstruction and PID efficiencies. The trigger, which performs the online data selection [27], consists of a hardware stage, based on the high transverse momentum, p_T , signatures from the calorimeter and muon systems, followed by a software stage with full event reconstruction. Two software trigger algorithms [13] are used to select candidates that are subsequently studied in separate categories because one of the triggers introduces a nontrivial efficiency dependence on the decay-time whereas the other has almost uniform decay-time efficiency.

The selection of $B_s^0 \rightarrow J/\psi(\rightarrow \mu^+ \mu^-) K^+ K^-$ candidates, with $K^+ K^-$ invariant masses in the range [990, 1050] MeV/c^2 , follows the same strategy used in the previous Run 2 measurement [13]. In order to take into account different data-taking and calibration conditions for optimal event selection, a gradient-boosted decision tree (BDT) classifier applied in the selection is trained separately for each year between 2016 and 2018, with the result for 2016 applied to the 2015 data set due to its limited size. The peaking backgrounds due to pion and proton misidentification in B^0 and Λ_b^0 decays are significantly reduced with stringent PID and mass requirements [13]. The remaining peaking background from $\Lambda_b^0 \rightarrow J/\psi p K^-$ decays is subtracted statistically through the injection of simulated events into the data with a negative sum of weights equal to the expected number of 4700 Λ_b^0 candidates.

Selected $B_s^0 \rightarrow J/\psi K^+ K^-$ candidates in the mass range [5200, 5550] MeV/c^2 are subsequently retained for analysis. The data sample is divided into 48 independent

¹The inclusion of charge-conjugate processes is implied throughout this paper, unless otherwise noted.

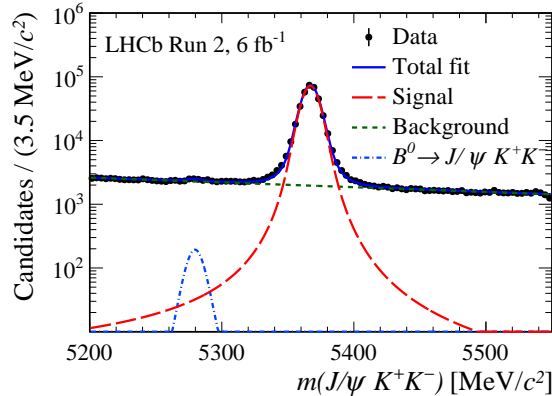


Figure 1: Distribution of $m(J/\psi K^+ K^-)$ for the full data sample and projection of the maximum likelihood fit.

subsamples, corresponding to six $m(K^+ K^-)$ bins with boundaries at 990, 1008, 1016, 1020, 1024, 1032 and 1050 MeV/c^2 , two trigger categories, and four years of data taking. The invariant mass of selected B_s^0 candidates, $m(J/\psi K^+ K^-)$, and the per-candidate mass uncertainty, σ_m , are calculated by constraining the J/ψ mass to the world average [20] and requiring the B_s^0 candidate momentum to point back to the corresponding primary vertex. Using $m(J/\psi K^+ K^-)$ as the discriminating variable, a signal weight is assigned to each candidate with the *sPlot* method [28–30], using an extended maximum-likelihood fit, shown in Fig. 1. The signal shape is described by a double-sided Crystal Ball function (CB) [31], whose width is parametrized as a function of σ_m , using a second-order polynomial. This parametrization [13] accounts for the correlation between $m(J/\psi K^+ K^-)$ and the helicity angle $\cos\theta_\mu$. The parameters that describe the tail of the CB function are fixed to those obtained from simulation. The background from $B^0 \rightarrow J/\psi K^+ K^-$ decays is modeled with the same CB function as the signal, sharing all shape parameters, except for the mean of the distribution. The difference between the means of the signal and B^0 components is fixed to its world average [20]. The background due to random combinations of tracks is modeled with an exponential function. The peaking background from $B^0 \rightarrow J/\psi K^+ \pi^-$ decays is estimated to be negligible. The $B_s^0 \rightarrow J/\psi K^+ K^-$ signal yields are $16\,181 \pm 135$, $103\,319 \pm 342$, $105\,465 \pm 343$ and $123\,870 \pm 476$ for the 2015, 2016, 2017 and 2018 datasets, respectively.

The measurement of ϕ_s in $B_s^0 \rightarrow J/\psi K^+ K^-$ decays requires the CP -even and CP -odd decay-amplitude components to be disentangled, depending upon the relative orbital angular momentum between the J/ψ candidate and the kaon pair. A weighted simultaneous fit to the distributions of decay time and decay angles ($\cos\theta_K, \cos\theta_\mu, \phi_h$) in the helicity basis, as described in Ref. [13], is performed to the 48 independent subsamples, to determine the physics parameters. These parameters are: ϕ_s ; $|\lambda|$; $\Gamma_s - \Gamma_d$; $\Delta\Gamma_s$; the B_s^0 mass difference, Δm_s ; and the polarization amplitudes $A_k = |A_k| e^{-i\delta_k}$, where the indices $k \in \{0, \parallel, \perp, S\}$ refer to the different polarization states of the $K^+ K^-$ system. The sum $|A_\parallel|^2 + |A_0|^2 + |A_\perp|^2$ equals unity and δ_0 is zero, by convention. The parameter λ , assumed to be the same for all polarization states, is defined as $\eta_k(q/p)(\bar{A}_k/A_k)$, where $p = \langle B_s^0 | B_L \rangle$ and $q = \langle \bar{B}_s^0 | B_L \rangle$ describe the relation between mass and flavor eigenstates and η_k is the CP eigenvalue of the polarization state k .

The probability density function (PDF) for the signal in each subsample accounts

for the decay-time resolution, the decay-time and angular efficiencies, and the flavor tagging. It considers P- and S-wave components of the kaon pair from $\phi(1020)$ and $f_0(980)$ decays, while the D-wave component is neglected [15, 32]. The interference of P- and S- wave includes an effective coupling factor, C_{SP} , determined in each $m(K^+K^-)$ bin through integration of the mass lineshape interference term. The lineshape of the $\phi(1020)$ resonance [15, 32] is modelled as a relativistic Breit–Wigner distribution, while the $f_0(980)$ resonance is modelled as a Flatté amplitude with parameters from Ref. [33]. The effect of mass resolution is also accounted for. The computed values of C_{SP} are 0.8458 ± 0.0018 , 0.8673 ± 0.0004 , 0.8127 ± 0.0012 , 0.8558 ± 0.0010 , 0.9359 ± 0.0004 and 0.9735 ± 0.0001 from the lowest to the highest $m(K^+K^-)$ bin. The value of Γ_d is fixed to its world average [34]. All physics parameters are left unconstrained in the fit and are shared across the subsamples, except for the S-wave fraction and the phase difference $\delta_{\text{S}} - \delta_{\perp}$, which are independent parameters for each $m(K^+K^-)$ bin.

The experimental decay-time resolution is accounted for by convolving the signal PDF with a Gaussian resolution function with the per-candidate decay-time uncertainty as the width. The per-candidate decay-time uncertainty is calibrated to represent the effective resolution, which is determined from a control sample of promptly decaying J/ψ candidates combined with two kaons selected similarly as the signal except for the decay time and flight distance requirements. The candidates with negative reconstructed decay times, arising from purely detector resolution effects, are used for the calibration. The average resolution for the signal candidates is determined to be around 42 fs.

The prompt sample used in the decay-time resolution calibration has a nonzero mean decay time due to residual detector misalignment. This bias, which depends on the kinematics, is corrected for in the analysis. In the misaligned simulated samples, a small bias remains after the correction and is assigned as a systematic uncertainty.

The reconstruction and selection produce a nonuniform efficiency as a function of the decay time and angles of the B_s^0 decays. The angular and decay-time efficiencies are assumed to factorize and are evaluated separately for different years of data taking and for the two trigger categories. The three-dimensional angular efficiency correction is introduced through normalization weights in the PDF describing the signal decays in the time-dependent angular fit. The efficiency is determined from simulated signal events subjected to the same selection criteria as data. The simulated sample is corrected by an iterative procedure using data [13].

The decay-time efficiency is determined using a data-driven method [13] with a reference channel $B^0 \rightarrow J/\psi K^{*0} (\rightarrow K^+\pi^-)$ that is topologically similar to the signal channel. The decay-time efficiency is modelled by a cubic spline function, with nodes at 0.30, 0.91, 1.96 and 9.00 ps, determined from the decay-time distribution of selected candidates divided by the expected distribution for the case of perfect acceptance. The latter is modelled by an exponential distribution with the B^0 lifetime, [20], convolved with a Gaussian resolution function with a width of 42 fs. Simulated B^0 and B_s^0 events are used to determine and apply corrections at the level of 3% to account for kinematic differences between B^0 and B_s^0 decays. The background-subtracted $B^0 \rightarrow J/\psi K^{*0}$ candidates are selected using the same strategy as in Ref. [13], with an additional requirement on the helicity angle $\cos\theta_K < 0$, to avoid a large difference between signal and control samples, since pions with $\cos\theta_K > 0$ tend to have extremely low momenta. The decay-time efficiency is validated by replacing B_s^0 samples with B^+ and B^0 samples where the decay widths are measured to be consistent with their corresponding world averages [20].

The flavor of the B_s^0 meson at production is inferred using two independent classes of flavor-tagging algorithms, the opposite-side (OS) tagger [35] and same-side (SS) tagger [36], which exploit specific accompanying B meson decays and signal fragmentation information, respectively. Each method yields a tagging decision Q , with an estimated mistag probability κ , for each B_s^0 meson, where $Q = +1, -1$ or 0 , if the meson is classified as B_s^0, \bar{B}_s^0 or untagged, respectively. To obtain the correct mistag probability ω , each algorithm is calibrated using a linear function following the same strategy as Ref. [13]. The calibration of the OS mistag probability uses $B^+ \rightarrow J/\psi K^+$ decays, for which the value of ω in an interval of κ can be obtained from the number of correct and wrong decisions. The calibration of the SS mistag probability uses flavor-specific $B_s^0 \rightarrow D_s^- \pi^+$ decays, for which the value of ω in an interval of κ is estimated by fitting the decay-time distribution. The decay-time acceptance is modeled with a cubic spline [37]. The effective tagging power is given by the product of the tagging efficiency (ϵ_{tag}) and the wrong-tag dilution squared, $\epsilon_{\text{tag}} \times (1 - 2\omega)^2$. The combined tagging powers of the OS and SS taggers are $(4.18 \pm 0.15)\%$, $(4.22 \pm 0.16)\%$, $(4.36 \pm 0.16)\%$ for 2015–2016, 2017 and 2018, where the statistical and systematic uncertainties are combined. A novel inclusive flavor-tagging algorithm [38], which uses track information from the full event, is applied as an alternative method to cross-check the OS and SS combined method and provides compatible results for ϕ_s with similar precision.

The results of the simultaneous maximum likelihood fit to the 48 independent data samples for the nine main physics parameters of interest are given in Table 1. The statistical uncertainties are computed using the profile-likelihood method and cross-checked with the bootstrapping technique [39, 40]. The background-subtracted data distributions with

Table 1: Main physics parameters of interest, where the first uncertainty is statistical and the second systematic.

Parameter	Values
ϕ_s [rad]	$-0.039 \pm 0.022 \pm 0.006$
$ \lambda $	$1.001 \pm 0.011 \pm 0.005$
$\Gamma_s - \Gamma_d$ [ps $^{-1}$]	$-0.0056 \begin{smallmatrix} +0.0013 \\ -0.0015 \end{smallmatrix} \pm 0.0014$
$\Delta\Gamma_s$ [ps $^{-1}$]	$0.0845 \pm 0.0044 \pm 0.0024$
Δm_s [ps $^{-1}$]	$17.743 \pm 0.033 \pm 0.009$
$ A_\perp ^2$	$0.2463 \pm 0.0023 \pm 0.0024$
$ A_0 ^2$	$0.5179 \pm 0.0017 \pm 0.0032$
$\delta_\perp - \delta_0$ [rad]	$2.903 \begin{smallmatrix} +0.075 \\ -0.074 \end{smallmatrix} \pm 0.048$
$\delta_\parallel - \delta_0$ [rad]	$3.146 \pm 0.061 \pm 0.052$

fit projections are shown in Fig. 2. The results are in good agreement with the LHCb Run 1 and 2015–2016 measurements [12–14]. As a cross-check, the analysis is performed on the 2015–2016 data subsample and the results are consistent with the previous Run 2 measurement [13]. The measurements of ϕ_s , $\Delta\Gamma_s$ and $\Gamma_s - \Gamma_d$ are the most precise to date and agree with the SM expectations [2, 41–43]. No CP violation in $B_s^0 \rightarrow J/\psi K^+ K^-$ decays is found. The value of Δm_s agrees with the world average [20]. The amplitudes of the S-wave component are determined in the same fit and summarized in the Supplemental Material [44]. Removing the assumption that the CP -violating parameters $|\lambda|$ and ϕ_s are

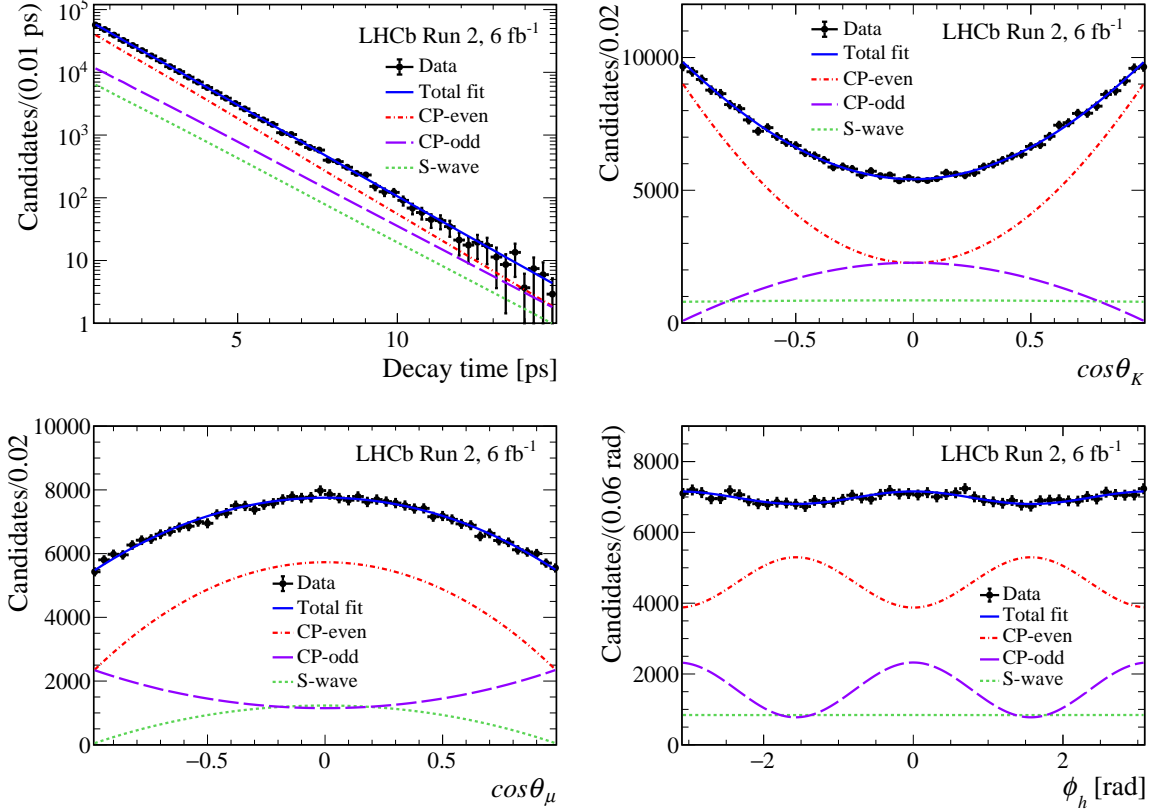


Figure 2: Decay-time and decay-angle distributions for background-subtracted $B_s^0 \rightarrow J/\psi K^+ K^-$ decays with the one-dimensional projections of the PDF at the maximum-likelihood point. The data and fit projections for the different samples considered (data-taking year, trigger and tagging categories, $m(K^+ K^-)$ bins) are combined.

the same for all polarization states shows no evidence for any polarization dependence, and the corresponding results are summarized in Table 2.

Table 2: Measured observables in the polarization-dependent fit. The uncertainties are statistical only.

Parameters	Values
ϕ_s^0 [rad]	-0.034 ± 0.023
$\phi_s^{\parallel} - \phi_s^0$ [rad]	-0.002 ± 0.021
$\phi_s^{\perp} - \phi_s^0$ [rad]	$-0.001^{+0.020}_{-0.021}$
$\phi_s^S - \phi_s^0$ [rad]	$0.022^{+0.027}_{-0.026}$
$ \lambda^0 $	$0.969^{+0.025}_{-0.024}$
$ \lambda^{\parallel}/\lambda^0 $	$0.982^{+0.055}_{-0.052}$
$ \lambda^{\perp}/\lambda^0 $	$1.107^{+0.082}_{-0.076}$
$ \lambda^S/\lambda^0 $	$1.121^{+0.084}_{-0.078}$

The total systematic uncertainties shown in Table 1 are the quadrature sum of different contributions, described in the following and summarized in the Supplemental Material [44].

The tagging parameters are constrained in the fit and therefore their associated systematic uncertainties contribute to the statistical uncertainty of each parameter. This contribution is 0.0025 rad to ϕ_s and 0.0015 ps⁻¹ to Δm_s and is negligible for all other parameters.

The systematic uncertainties related to the mass fit model are estimated by changing the calibration model of the per-candidate mass uncertainty, varying the estimation of misidentified A_b^0 and mass resolution parameters independently. The signal weights are recomputed by varying the fit parameters within their statistical uncertainties. Since the *sPlot* method implicitly relies on factorization of the discriminating variable, $m(J/\psi K^+ K^-)$, and the rest of the observables, a systematic uncertainty is assigned for the small correlation between the $m(J/\psi K^+ K^-)$ distribution and the decay time and angles by reevaluating the signal weights in bins of decay time and angles. The effect of ignoring the contribution of $B_c^+ \rightarrow B_s^0 X$ candidates is evaluated with pseudoexperiments by adding about 2% [45–47] of $B_c^+ \rightarrow B_s^0(\rightarrow J/\psi\phi)X$ simulated candidates, estimated from the branching fraction and efficiencies. The B_c^+ component causes biases in Γ_s and $\Delta\Gamma_s$ at the level of about 0.0015 ps⁻¹. These are corrected for in the final fit, while minor differences in other parameters are taken as systematic uncertainties. The effect of neglecting a possible D-wave $K^+ K^-$ component is conservatively estimated with pseudoexperiments that contain twice the size of the expected D-wave contribution from Ref. [32].

The effect due to imperfect removal of ghost tracks [48] reconstructed with noisy hits is evaluated according to simulation and considered among the systematic uncertainties. Around 1.4% of the selected events have multiple candidates; the effect of such cases is considered in systematic uncertainties by choosing one candidate randomly and repeating the fit. Systematic uncertainties are assigned due to the limited size of the PID calibration samples. Different models of the S-wave lineshape based on the results in Ref. [33] are used to evaluate the C_{SP} factors and assign systematic uncertainties.

A systematic uncertainty for the translation of the decay-time resolution calibration from the control sample to signal is derived using simulation. A minor systematic uncertainty due to non-Gaussian effects in the decay-time resolution is assigned. A systematic uncertainty accounting for the limited size of the calibration sample is assigned considering correlations among the parameters. The effect of limited size of simulated samples for the determination of the angular efficiency is estimated by varying the efficiency according to the statistical covariance matrix. The effect of ignoring the angular resolutions in the fit is estimated by performing separate fits to the generated and reconstructed variables from simulation, and the differences are taken as systematic uncertainties. The effect of the specific configuration of the gradient-boosted tree method applied to correct the kinematics of simulation in the time and angular efficiency is estimated applying 100 alternative configurations.

The longitudinal scale of the vertex detector has a relative uncertainty of 0.022% [49,50] and a systematic uncertainty is assigned by scaling the track parameters with this uncertainty. The systematic uncertainty associated with the track momentum scale calibration is estimated by varying all track momenta by 0.03% [51]. Possible biases in the fitting procedure and effects of neglecting correlations between the decay-angle and decay-time efficiencies are studied using pseudoexperiments. The results are found to be stable when repeating the analysis on subsets of the data, split by the two LHCb magnet polarities, trigger conditions, year of data taking, number of reconstructed primary vertices, bins of $B_s^0 p_T$, η or tagging categories.

In conclusion, the CP -violation and decay-width parameters in the decay

$B_s^0 \rightarrow J/\psi K^+ K^-$ are measured using the full Run 2 data set collected by the LHCb experiment. The results are $\phi_s = -0.039 \pm 0.022 \pm 0.006$ rad, $|\lambda| = 1.001 \pm 0.011 \pm 0.005$, $\Gamma_s - \Gamma_d = -0.0056_{-0.0015}^{+0.0013} \pm 0.0014$ ps $^{-1}$ and $\Delta\Gamma_s = 0.0845 \pm 0.0044 \pm 0.0024$ ps $^{-1}$, superseding the previous Run 2 LHCb measurement in the same decay [13]. No evidence for CP violation is found in the $B_s^0 \rightarrow J/\psi(\mu^+\mu^-)K^+K^-$ decay. The results are consistent with the previous measurements in $B_s^0 \rightarrow J/\psi(\mu^+\mu^-)K^+K^-$ [12, 13] and $B_s^0 \rightarrow J/\psi(e^+e^-)K^+K^-$ [14] decays, and the combination with which yields $\phi_s = -0.044 \pm 0.020$ rad and $|\lambda| = 0.990 \pm 0.010$. A combination of all LHCb ϕ_s measurements in B_s^0 decays via $b \rightarrow c\bar{c}s$ transitions [12, 14–16, 18, 19], $B_s^0 \rightarrow J/\psi(\mu^+\mu^-)K^+K^-$ above the $\phi(1020)$ resonance, $B_s^0 \rightarrow D_s^+ D_s^-$, $B_s^0 \rightarrow J/\psi\pi^+\pi^-$, $B_s^0 \rightarrow \psi(2S)K^+K^-$ and $B_s^0 \rightarrow J/\psi K^+K^-$, yields $\phi_s = -0.031 \pm 0.018$ rad. The full fit results and correlations are provided in the Supplemental Material [44]. This is the most precise measurement of the CP -violating phase ϕ_s to date and is consistent with SM predictions [2, 41].

Acknowledgements

We express our gratitude to our colleagues in the CERN accelerator departments for the excellent performance of the LHC. We thank the technical and administrative staff at the LHCb institutes. We acknowledge support from CERN and from the national agencies: CAPES, CNPq, FAPERJ and FINEP (Brazil); MOST and NSFC (China); CNRS/IN2P3 (France); BMBF, DFG and MPG (Germany); INFN (Italy); NWO (Netherlands); MNiSW and NCN (Poland); MCID/IFA (Romania); MICINN (Spain); SNSF and SER (Switzerland); NASU (Ukraine); STFC (United Kingdom); DOE NP and NSF (USA). We acknowledge the computing resources that are provided by CERN, IN2P3 (France), KIT and DESY (Germany), INFN (Italy), SURF (Netherlands), PIC (Spain), GridPP (United Kingdom), CSCS (Switzerland), IFIN-HH (Romania), CBPF (Brazil), Polish WLCG (Poland) and NERSC (USA). We are indebted to the communities behind the multiple open-source software packages on which we depend. Individual groups or members have received support from ARC and ARDC (Australia); Minciencias (Colombia); AvH Foundation (Germany); EPLANET, Marie Skłodowska-Curie Actions, ERC and NextGenerationEU (European Union); A*MIDEX, ANR, IPhU and Labex P2IO, and Région Auvergne-Rhône-Alpes (France); Key Research Program of Frontier Sciences of CAS, CAS PIFI, CAS CCEPP, Fundamental Research Funds for the Central Universities, and Sci. & Tech. Program of Guangzhou (China); GVA, XuntaGal, GENCAT, Inditex, InTalent and Prog. Atracción Talento, CM (Spain); SRC (Sweden); the Leverhulme Trust, the Royal Society and UKRI (United Kingdom).


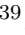
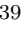















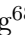


























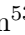




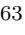






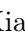
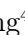




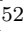

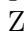



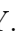
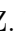



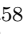


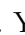
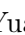

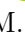




















References

- [1] M. Kobayashi and T. Maskawa, *CP-violation in the renormalizable theory of weak interaction*, Prog. Theor. Phys. **49** (1973) 652; N. Cabibbo, *Unitary symmetry and leptonic decays*, Phys. Rev. Lett. **10** (1963) 531.
- [2] CKMfitter group, J. Charles *et al.*, *Current status of the standard model CKM fit and constraints on $\Delta F = 2$ new physics*, Phys. Rev. **D91** (2015) 073007, arXiv:1501.05013, updated results and plots available at <http://ckmfitter.in2p3.fr/>.
- [3] A. J. Buras, *Flavour theory: 2009*, PoS **EPS-HEP2009** (2009) 024, arXiv:0910.1032.
- [4] B. Dutta and Y. Mimura, *Large phase of B_s^0 - \bar{B}_s^0 mixing in Supersymmetric Grand Unified Theories*, Phys. Rev. **D78** (2008) 071702, arXiv:0805.2988.
- [5] CDF collaboration, T. Aaltonen *et al.*, *Measurement of the bottom-strange meson mixing phase in the full CDF data set*, Phys. Rev. Lett. **109** (2012) 171802, arXiv:1208.2967.
- [6] D0 collaboration, V. M. Abazov *et al.*, *Measurement of the CP-violating phase $\phi_s^{J/\psi\phi}$ using the flavor-tagged decay $B_s^0 \rightarrow J/\psi\phi$ in 8 fb^{-1} of $p\bar{p}$ collisions*, Phys. Rev. **D85** (2012) 032006, arXiv:1109.3166.
- [7] ATLAS collaboration, G. Aad *et al.*, *Flavour tagged time dependent angular analysis of the $B_s \rightarrow J/\psi\phi$ decay and extraction of $\Delta\Gamma_s$ and the weak phase ϕ_s in ATLAS*, Phys. Rev. **D90** (2014) 052007, arXiv:1407.1796.
- [8] ATLAS collaboration, G. Aad *et al.*, *Measurement of the CP-violating phase ϕ_s and the B_s^0 meson decay width difference with $B_s^0 \rightarrow J/\psi\phi$ decays in ATLAS*, JHEP **08** (2016) 147, arXiv:1601.03297.
- [9] ATLAS collaboration, G. Aad *et al.*, *Measurement of the CP-violating phase ϕ_s in $B_s^0 \rightarrow J/\psi\phi$ decays in ATLAS at 13 TeV*, Eur. Phys. J. **C81** (2021) 342, arXiv:2001.07115.
- [10] CMS collaboration, V. Khachatryan *et al.*, *Measurement of the CP-violating weak phase ϕ_s and the decay width difference $\Delta\Gamma_s$ using the $B_s^0 \rightarrow J/\psi\phi(1020)$ decay channel in pp collisions at $\sqrt{s} = 8 \text{ TeV}$* , Phys. Lett. **B757** (2016) 97, arXiv:1507.07527.
- [11] CMS collaboration, A. M. Sirunyan *et al.*, *Measurement of the CP-violating phase ϕ_s in the $B_s^0 \rightarrow J/\psi\phi(1020) \rightarrow \mu^+\mu^-K^+K^-$ channel in proton-proton collisions at $\sqrt{s} = 13 \text{ TeV}$* , Phys. Lett. **B816** (2021) 136188, arXiv:2007.02434.
- [12] LHCb collaboration, R. Aaij *et al.*, *Precision measurement of CP violation in $B_s^0 \rightarrow J/\psi K^+K^-$ decays*, Phys. Rev. Lett. **114** (2015) 041801, arXiv:1411.3104.
- [13] LHCb collaboration, R. Aaij *et al.*, *Updated measurement of time-dependent CP-violating observables in $B_s^0 \rightarrow J/\psi K^+K^-$ decays*, Eur. Phys. J. **C79** (2019) 706, Erratum *ibid.* **C80** (2020) 601, arXiv:1906.08356.

- [14] LHCb collaboration, R. Aaij *et al.*, *First measurement of the CP-violating phase in $B_s^0 \rightarrow J/\psi(e^+e^-)\phi$ decays*, arXiv:2105.14738, to appear in EPJC.
- [15] LHCb collaboration, R. Aaij *et al.*, *Resonances and CP-violation in B_s^0 and $\bar{B}_s^0 \rightarrow J/\psi K^+ K^-$ decays in the mass region above the $\phi(1020)$* , JHEP **08** (2017) 037, arXiv:1704.08217.
- [16] LHCb collaboration, R. Aaij *et al.*, *Measurement of the CP-violating phase ϕ_s in $\bar{B}_s^0 \rightarrow J/\psi\pi^+\pi^-$ decays*, Phys. Lett. **B736** (2014) 186, arXiv:1405.4140.
- [17] LHCb collaboration, R. Aaij *et al.*, *Measurement of the CP-violating phase ϕ_s from $B_s^0 \rightarrow J/\psi\pi^+\pi^-$ decays in 13 TeV pp collisions*, Phys. Lett. **B797** (2019) 134789, arXiv:1903.05530.
- [18] LHCb collaboration, R. Aaij *et al.*, *Measurement of the CP violating phase and decay-width difference in $B_s^0 \rightarrow \psi(2S)\phi$ decays*, Phys. Lett. **B762** (2016) 253, arXiv:1608.04855.
- [19] LHCb collaboration, R. Aaij *et al.*, *Measurement of the CP-violating phase ϕ_s in $\bar{B}_s^0 \rightarrow D_s^+ D_s^-$ decays*, Phys. Rev. Lett. **113** (2014) 211801, arXiv:1409.4619.
- [20] Particle Data Group, R. L. Workman *et al.*, *Review of particle physics*, Prog. Theor. Exp. Phys. **2022** (2022) 083C01.
- [21] LHCb collaboration, A. A. Alves Jr. *et al.*, *The LHCb detector at the LHC*, JINST **3** (2008) S08005.
- [22] LHCb collaboration, R. Aaij *et al.*, *LHCb detector performance*, Int. J. Mod. Phys. **A30** (2015) 1530022, arXiv:1412.6352.
- [23] T. Sjöstrand, S. Mrenna, and P. Skands, *A brief introduction to PYTHIA 8.1*, Comput. Phys. Commun. **178** (2008) 852, arXiv:0710.3820; T. Sjöstrand, S. Mrenna, and P. Skands, *PYTHIA 6.4 physics and manual*, JHEP **05** (2006) 026, arXiv:hep-ph/0603175.
- [24] I. Belyaev *et al.*, *Handling of the generation of primary events in Gauss, the LHCb simulation framework*, J. Phys. Conf. Ser. **331** (2011) 032047.
- [25] D. J. Lange, *The EvtGen particle decay simulation package*, Nucl. Instrum. Meth. **A462** (2001) 152.
- [26] N. Davidson, T. Przedzinski, and Z. Was, *PHOTOS interface in C++: Technical and physics documentation*, Comp. Phys. Comm. **199** (2016) 86, arXiv:1011.0937.
- [27] R. Aaij *et al.*, *The LHCb trigger and its performance in 2011*, JINST **8** (2013) P04022, arXiv:1211.3055.
- [28] M. Pivk and F. R. L. Diberder, *sPlot: a statistical tool to unfold data distributions*, Nucl. Instrum. Meth. **A555** (2005) 356, arXiv:physics/0402083.
- [29] Y. Xie, *sFit: A method for background subtraction in maximum likelihood fit*, arXiv:0905.0724.

- [30] H. Dembinski, M. Kenzie, C. Langenbruch, and M. Schmelling, *Custom orthogonal weight functions (COWs) for event classification*, Nucl. Instrum. Meth. **A1040** (2022) 167270.
- [31] T. Skwarnicki, *A study of the radiative cascade transitions between the Upsilon-prime and Upsilon resonances*, PhD thesis, Institute of Nuclear Physics, Krakow, 1986, DESY-F31-86-02.
- [32] LHCb collaboration, R. Aaij *et al.*, *Amplitude analysis and branching fraction measurement of $\bar{B}_s^0 \rightarrow J/\psi K^+ K^-$* , Phys. Rev. **D87** (2013) 072004, arXiv:1302.1213.
- [33] LHCb collaboration, R. Aaij *et al.*, *Measurement of resonant and CP components in $\bar{B}_s^0 \rightarrow J/\psi \pi^+ \pi^-$ decays*, Phys. Rev. **D89** (2014) 092006, arXiv:1402.6248.
- [34] Heavy Flavor Averaging Group, Y. Amhis *et al.*, *Averages of b-hadron, c-hadron, and τ -lepton properties as of 2021*, Phys. Rev. **D107** (2023) 052008.
- [35] LHCb collaboration, R. Aaij *et al.*, *Opposite-side flavour tagging of B mesons at the LHCb experiment*, Eur. Phys. J. **C72** (2012) 2022, arXiv:1202.4979.
- [36] LHCb collaboration, R. Aaij *et al.*, *A new algorithm for identifying the flavour of B_s^0 mesons at LHCb*, JINST **11** (2016) P05010, arXiv:1602.07252.
- [37] LHCb collaboration, R. Aaij *et al.*, *Precise determination of the $B_s^0 - \bar{B}_s^0$ oscillation frequency*, Nature Physics **18** (2022) 1, arXiv:2104.04421.
- [38] T. Likhomanenko, D. Derkach, A. Rogozhnikov, *Inclusive flavour tagging algorithm*, J. Phys. : Conf. Ser. **762** (2016) 012045, arXiv:1705.08707.
- [39] B. Efron, *Bootstrap Methods: Another look at the Jackknife*, The Annals of Statistics **7** (1979) 1 .
- [40] C. Langenbruch, *Parameter uncertainties in weighted unbinned maximum likelihood fits*, Eur. Phys. J. **C82** (2022) 393, arXiv:1911.01303.
- [41] UTfit collaboration, M. Bona *et al.*, *The unitarity triangle fit in the standard model and hadronic parameters from lattice QCD: A reappraisal after the measurements of Δm_s and $BR(B \rightarrow \tau \nu_\tau)$* , JHEP **10** (2006) 081, arXiv:hep-ph/0606167, updated results and plots available at <http://www.utfit.org/>.
- [42] M. Artuso, G. Borissov, and A. Lenz, *CP violation in the B_s^0 system*, Rev. Mod. Phys. **88** (2016) 045002, arXiv:1511.09466.
- [43] M. Kirk, A. Lenz, and T. Rauh, *Dimension-six matrix elements for meson mixing and lifetimes from sum rules*, JHEP **12** (2017) 068, arXiv:1711.02100.
- [44] *See Supplemental Material at [link inserted by publisher] for a summary of systematic uncertainties and numerical results and additional plots for the fit result and combinations of LHCb measurement.*
- [45] LHCb collaboration, R. Aaij *et al.*, *Measurement of the B_c^- production fraction and asymmetry in 7 and 13 TeV pp collisions*, Phys. Rev. **D100** (2019) 112006, arXiv:1910.13404.

- [46] LHCb collaboration, R. Aaij *et al.*, *Precise measurement of the f_s/f_d ratio of fragmentation fractions and of B_s^0 decay branching fractions*, Phys. Rev. **D104** (2021) 032005, [arXiv:2103.06810](#).
- [47] V. V. Kiselev, *Decays of the B_c meson*, [arXiv:hep-ph/0308214](#).
- [48] P. Li, E. Rodrigues, and S. Stahl, *Tracking Definitions and Conventions for Run 3 and Beyond*, LHCb-PUB-2021-005, CERN-LHCb-PUB-2021-005, 2021.
- [49] R. Aaij *et al.*, *Performance of the LHCb Vertex Locator*, JINST **9** (2014) P09007, [arXiv:1405.7808](#).
- [50] LHCb collaboration, R. Aaij *et al.*, *Precision measurement of the $B_s^0-\bar{B}_s^0$ oscillation frequency in the decay $B_s^0 \rightarrow D_s^- \pi^+$* , New J. Phys. **15** (2013) 053021, [arXiv:1304.4741](#).
- [51] LHCb collaboration, M. Needham, *Momentum scale calibration using resonances*, CERN-LHCb-2008-037, 2008.

D. vom Bruch¹¹ , V. Vorobyev³⁹ , N. Voropaev³⁹ , K. Vos⁷⁶ , C. Vrahas⁵⁴ , J. Walsh³⁰ , E.J. Walton⁶⁵ , G. Wan⁵ , C. Wang¹⁸ , G. Wang⁷ , J. Wang⁵ , J. Wang⁴ , J. Wang³ , J. Wang⁷⁰ , M. Wang²⁶ , N. W. Wang⁶ , R. Wang⁵⁰ , X. Wang⁶⁸ , Y. Wang⁷ , Z. Wang⁴⁶ , Z. Wang³ , Z. Wang⁶ , J.A. Ward^{52,65} , N.K. Watson⁴⁹ , D. Websdale⁵⁷ , Y. Wei⁵ , B.D.C. Westhenry⁵⁰ , D.J. White⁵⁸ , M. Whitehead⁵⁵ , A.R. Wiederhold⁵² , D. Wiedner¹⁶ , G. Wilkinson⁵⁹ , M.K. Wilkinson⁶¹ , I. Williams⁵¹ , M. Williams⁶⁰ , M.R.J. Williams⁵⁴ , R. Williams⁵¹ , F.F. Wilson⁵³ , W. Wislicki³⁷ , M. Witek³⁶ , L. Witola¹⁸ , C.P. Wong⁶³ , G. Wormser¹² , S.A. Wotton⁵¹ , H. Wu⁶⁴ , J. Wu⁷ , Y. Wu⁵ , K. Wyllie⁴⁴ , S. Xian⁶⁸ , Z. Xiang⁴ , Y. Xie⁷ , A. Xu³⁰ , J. Xu⁶ , L. Xu³ , L. Xu³ , M. Xu⁵² , Z. Xu¹⁰ , Z. Xu⁶ , Z. Xu⁴ , D. Yang³ , S. Yang⁶ , X. Yang⁵ , Y. Yang²⁵ , Z. Yang⁵ , Z. Yang⁶² , V. Yeroshenko¹² , H. Yeung⁵⁸ , H. Yin⁷ , C. Y. Yu⁵ , J. Yu⁶⁷ , X. Yuan⁴ , E. Zaffaroni⁴⁵ , M. Zavertyaev¹⁷ , M. Zdybal³⁶ , M. Zeng³ , C. Zhang⁵ , D. Zhang⁷ , J. Zhang⁶ , L. Zhang³ , S. Zhang⁶⁷ , S. Zhang⁵ , Y. Zhang⁵ , Y. Zhang⁵⁹ , Y. Zhao¹⁸ , A. Zharkova³⁹ , A. Zhelezov¹⁸ , Y. Zheng⁶ , T. Zhou⁵ , X. Zhou⁷ , Y. Zhou⁶ , V. Zhovkovska¹² , L. Z. Zhu⁶ , X. Zhu³ , X. Zhu⁷ , Z. Zhu⁶ , V. Zhukov^{15,39} , J. Zhuo⁴³ , Q. Zou^{4,6} , S. Zucchelli^{21,j} , D. Zuliani²⁹ , G. Zunica⁵⁸ .

¹ *Centro Brasileiro de Pesquisas Físicas (CBPF), Rio de Janeiro, Brazil*

² *Universidade Federal do Rio de Janeiro (UFRJ), Rio de Janeiro, Brazil*

³ *Center for High Energy Physics, Tsinghua University, Beijing, China*

⁴ *Institute Of High Energy Physics (IHEP), Beijing, China*

⁵ *School of Physics State Key Laboratory of Nuclear Physics and Technology, Peking University, Beijing, China*

⁶ *University of Chinese Academy of Sciences, Beijing, China*

⁷ *Institute of Particle Physics, Central China Normal University, Wuhan, Hubei, China*

⁸ *Consejo Nacional de Rectores (CONARE), San Jose, Costa Rica*

⁹ *Université Savoie Mont Blanc, CNRS, IN2P3-LAPP, Annecy, France*

¹⁰ *Université Clermont Auvergne, CNRS/IN2P3, LPC, Clermont-Ferrand, France*

¹¹ *Aix Marseille Univ, CNRS/IN2P3, CPPM, Marseille, France*

¹² *Université Paris-Saclay, CNRS/IN2P3, IJCLab, Orsay, France*

¹³ *Laboratoire Leprince-Ringuet, CNRS/IN2P3, Ecole Polytechnique, Institut Polytechnique de Paris, Palaiseau, France*

¹⁴ *LPNHE, Sorbonne Université, Paris Diderot Sorbonne Paris Cité, CNRS/IN2P3, Paris, France*

¹⁵ *I. Physikalisches Institut, RWTH Aachen University, Aachen, Germany*

¹⁶ *Fakultät Physik, Technische Universität Dortmund, Dortmund, Germany*

¹⁷ *Max-Planck-Institut für Kernphysik (MPIK), Heidelberg, Germany*

¹⁸ *Physikalisches Institut, Ruprecht-Karls-Universität Heidelberg, Heidelberg, Germany*

¹⁹ *School of Physics, University College Dublin, Dublin, Ireland*

²⁰ *INFN Sezione di Bari, Bari, Italy*

²¹ *INFN Sezione di Bologna, Bologna, Italy*

²² *INFN Sezione di Ferrara, Ferrara, Italy*

²³ *INFN Sezione di Firenze, Firenze, Italy*

²⁴ *INFN Laboratori Nazionali di Frascati, Frascati, Italy*

²⁵ *INFN Sezione di Genova, Genova, Italy*

²⁶ *INFN Sezione di Milano, Milano, Italy*

²⁷ *INFN Sezione di Milano-Bicocca, Milano, Italy*

²⁸ *INFN Sezione di Cagliari, Monserrato, Italy*

²⁹ *Università degli Studi di Padova, Università e INFN, Padova, Padova, Italy*

³⁰ *INFN Sezione di Pisa, Pisa, Italy*

³¹ *INFN Sezione di Roma La Sapienza, Roma, Italy*

³² *INFN Sezione di Roma Tor Vergata, Roma, Italy*

³³ *Nikhef National Institute for Subatomic Physics, Amsterdam, Netherlands*

³⁴ *Nikhef National Institute for Subatomic Physics and VU University Amsterdam, Amsterdam, Netherlands*

- ³⁵ *AGH - University of Science and Technology, Faculty of Physics and Applied Computer Science, Kraków, Poland*
- ³⁶ *Henryk Niewodniczanski Institute of Nuclear Physics Polish Academy of Sciences, Kraków, Poland*
- ³⁷ *National Center for Nuclear Research (NCBJ), Warsaw, Poland*
- ³⁸ *Horia Hulubei National Institute of Physics and Nuclear Engineering, Bucharest-Magurele, Romania*
- ³⁹ *Affiliated with an institute covered by a cooperation agreement with CERN*
- ⁴⁰ *DS4DS, La Salle, Universitat Ramon Llull, Barcelona, Spain*
- ⁴¹ *ICCUB, Universitat de Barcelona, Barcelona, Spain*
- ⁴² *Instituto Galego de Física de Altas Enerxías (IGFAE), Universidade de Santiago de Compostela, Santiago de Compostela, Spain*
- ⁴³ *Instituto de Física Corpuscular, Centro Mixto Universidad de Valencia - CSIC, Valencia, Spain*
- ⁴⁴ *European Organization for Nuclear Research (CERN), Geneva, Switzerland*
- ⁴⁵ *Institute of Physics, Ecole Polytechnique Fédérale de Lausanne (EPFL), Lausanne, Switzerland*
- ⁴⁶ *Physik-Institut, Universität Zürich, Zürich, Switzerland*
- ⁴⁷ *NSC Kharkiv Institute of Physics and Technology (NSC KIPT), Kharkiv, Ukraine*
- ⁴⁸ *Institute for Nuclear Research of the National Academy of Sciences (KINR), Kyiv, Ukraine*
- ⁴⁹ *University of Birmingham, Birmingham, United Kingdom*
- ⁵⁰ *H.H. Wills Physics Laboratory, University of Bristol, Bristol, United Kingdom*
- ⁵¹ *Cavendish Laboratory, University of Cambridge, Cambridge, United Kingdom*
- ⁵² *Department of Physics, University of Warwick, Coventry, United Kingdom*
- ⁵³ *STFC Rutherford Appleton Laboratory, Didcot, United Kingdom*
- ⁵⁴ *School of Physics and Astronomy, University of Edinburgh, Edinburgh, United Kingdom*
- ⁵⁵ *School of Physics and Astronomy, University of Glasgow, Glasgow, United Kingdom*
- ⁵⁶ *Oliver Lodge Laboratory, University of Liverpool, Liverpool, United Kingdom*
- ⁵⁷ *Imperial College London, London, United Kingdom*
- ⁵⁸ *Department of Physics and Astronomy, University of Manchester, Manchester, United Kingdom*
- ⁵⁹ *Department of Physics, University of Oxford, Oxford, United Kingdom*
- ⁶⁰ *Massachusetts Institute of Technology, Cambridge, MA, United States*
- ⁶¹ *University of Cincinnati, Cincinnati, OH, United States*
- ⁶² *University of Maryland, College Park, MD, United States*
- ⁶³ *Los Alamos National Laboratory (LANL), Los Alamos, NM, United States*
- ⁶⁴ *Syracuse University, Syracuse, NY, United States*
- ⁶⁵ *School of Physics and Astronomy, Monash University, Melbourne, Australia, associated to ⁵²*
- ⁶⁶ *Pontifícia Universidade Católica do Rio de Janeiro (PUC-Rio), Rio de Janeiro, Brazil, associated to ²*
- ⁶⁷ *Physics and Micro Electronic College, Hunan University, Changsha City, China, associated to ⁷*
- ⁶⁸ *Guangdong Provincial Key Laboratory of Nuclear Science, Guangdong-Hong Kong Joint Laboratory of Quantum Matter, Institute of Quantum Matter, South China Normal University, Guangzhou, China, associated to ³*
- ⁶⁹ *Lanzhou University, Lanzhou, China, associated to ⁴*
- ⁷⁰ *School of Physics and Technology, Wuhan University, Wuhan, China, associated to ³*
- ⁷¹ *Departamento de Física, Universidad Nacional de Colombia, Bogotá, Colombia, associated to ¹⁴*
- ⁷² *Universität Bonn - Helmholtz-Institut für Strahlen und Kernphysik, Bonn, Germany, associated to ¹⁸*
- ⁷³ *Eotvos Lorand University, Budapest, Hungary, associated to ⁴⁴*
- ⁷⁴ *INFN Sezione di Perugia, Perugia, Italy, associated to ²²*
- ⁷⁵ *Van Swinderen Institute, University of Groningen, Groningen, Netherlands, associated to ³³*
- ⁷⁶ *Universiteit Maastricht, Maastricht, Netherlands, associated to ³³*
- ⁷⁷ *Tadeusz Kosciuszko Cracow University of Technology, Cracow, Poland, associated to ³⁶*
- ⁷⁸ *Department of Physics and Astronomy, Uppsala University, Uppsala, Sweden, associated to ⁵⁵*
- ⁷⁹ *University of Michigan, Ann Arbor, MI, United States, associated to ⁶⁴*
- ⁸⁰ *Departement de Physique Nucleaire (SPhN), Gif-Sur-Yvette, France*

^a *Universidade de Brasília, Brasília, Brazil*

^b *Centro Federal de Educação Tecnológica Celso Suckow da Fonseca, Rio De Janeiro, Brazil*

^c *Universidade Federal do Triângulo Mineiro (UFTM), Uberaba-MG, Brazil*

^d *Central South U., Changsha, China*

^e *Hangzhou Institute for Advanced Study, UCAS, Hangzhou, China*

^f *LIP6, Sorbonne Universite, Paris, France*

- ^g *Excellence Cluster ORIGINS, Munich, Germany*
- ^h *Universidad Nacional Autónoma de Honduras, Tegucigalpa, Honduras*
- ⁱ *Università di Bari, Bari, Italy*
- ^j *Università di Bologna, Bologna, Italy*
- ^k *Università di Cagliari, Cagliari, Italy*
- ^l *Università di Ferrara, Ferrara, Italy*
- ^m *Università di Firenze, Firenze, Italy*
- ⁿ *Università di Genova, Genova, Italy*
- ^o *Università degli Studi di Milano, Milano, Italy*
- ^p *Università di Milano Bicocca, Milano, Italy*
- ^q *Università di Padova, Padova, Italy*
- ^r *Università di Perugia, Perugia, Italy*
- ^s *Scuola Normale Superiore, Pisa, Italy*
- ^t *Università di Pisa, Pisa, Italy*
- ^u *Università della Basilicata, Potenza, Italy*
- ^v *Università di Roma Tor Vergata, Roma, Italy*
- ^w *Università di Urbino, Urbino, Italy*
- ^x *Universidad de Alcalá, Alcalá de Henares, Spain*
- ^y *Universidade da Coruña, Coruña, Spain*
- [†] *Deceased*